PROGRESS ON HELICON WAVE SOURCES

F.F. Chen, I.D. Sudit, M.E. Light, D.D. Blackwell, D.W. Aossey, D. Arnush, and A. Peskoff

University of California, Los Angeles, CA 90024-1594

Abstract: Because of their high ionization efficiency, helicon wave discharges are prime candidates for future industrial plasma sources used in semiconductor and flat-panel display manufacturing. This paper summarizes a large number of theoretical and experimental results on the physics and optimization of these devices.

1. Helicon waves in nonuniform plasmas [1]. The theory of helicon waves has been extended to plasmas with an arbitrary radial density profile $p(r) = n_0(r)/n_0$. When the radial wave equation is expressed in terms of the axial component B_z of the wave magnetic field, a singularity in the coefficients of the equation requires careful numerical treatment. When expressed in terms of the radial component B_r, however, the equation for waves of the form $\exp[i(m\theta - kz - \omega t)]$ is regular:

$$B_r'' + \left(1 + \frac{2m^2}{m^2 + \lambda k^2 r^2}\right)\frac{B_r'}{r} - \left[m^2 + \frac{mr\alpha}{k\lambda}\frac{\alpha'}{\alpha} - \frac{r^2}{\lambda}(\alpha^2 - k^2\lambda^2) - \frac{m^2 - kr^2(2m\alpha - k\lambda)}{m^2 + \lambda k^2 r^2}\right]\frac{B_r}{r^2} = 0, \quad (1)$$

where $\lambda \equiv 1 - (\omega/ck)^2$ and $\alpha(r) = \dfrac{\omega}{k}\dfrac{e\mu_0}{B_0}n_0(r)$. (2)

Eq. (1) has been integrated numerically for profiles of the form $p(r) = [1 - (r/a)^s]^t$. Fig. 1 shows the magnetic (solid) and electric (dashed) field lines for a parabolic profile, s =2, t =1.

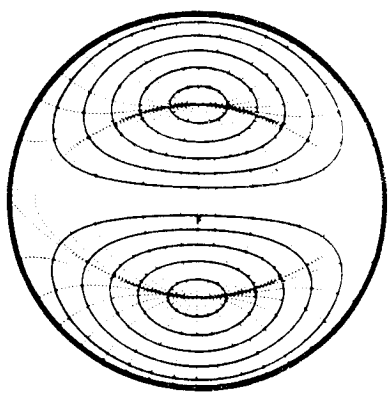

Fig. 1a (m = +1)

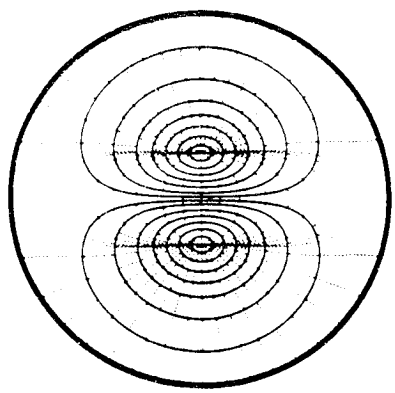

Fig. 1b (m = -1)

We see that the left-hand polarized (m = -1) mode is more concentrated near the axis than the right-hand (m = +1) mode and should lead to less uniform plasmas with a high peak density.

2. Wave excitation by straight and helical antennas [2]. The r, θ, *and* z components of the wave B-field have been measured using single-turn, coaxial magnetic probes for right-hand helical, left-hand helical, and plane-polarized Nagoya Type III antennas. Fig. 2 shows the radial variation of B_θ for these half-wavelength antennas. The curves are for the m = +1 (solid)

1994 INTERNATIONAL CONFERENCE ON PLASMA PHYSICS

Combined with

VI LATIN AMERICAN WORKSHOP ON PLASMA PHYSICS

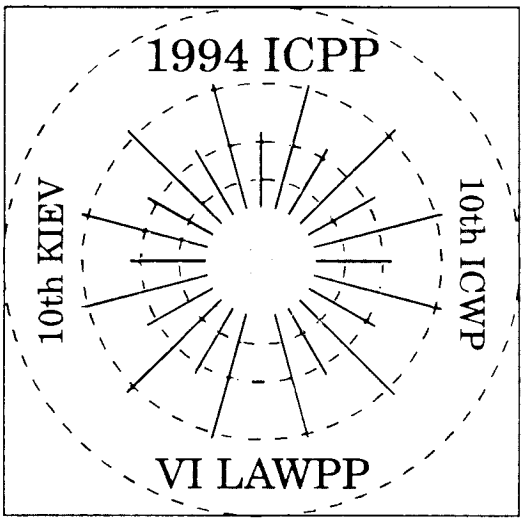

Proceedings

Contributed Papers

Editors: P.H. Sakanaka
E.Del Bosco
M.V. Alves

FOZ DO IGUAÇU - PR - BRAZIL

October 31 - November 4, 1994

VOLUME 3

and m = -1 (dashed) modes, computed from Eq. (1) using the measured $p(r)$. We see that the m = +1 mode is preferentially excited in all cases, even with the left-hand antenna. Bifilar antennas with giving rotating fields are needed for better mode control.

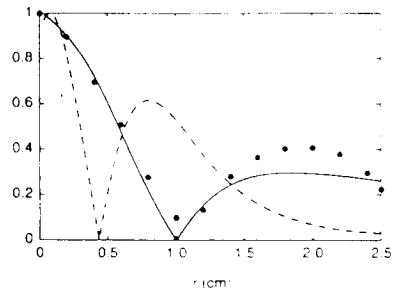

Fig. 2a R-antenna

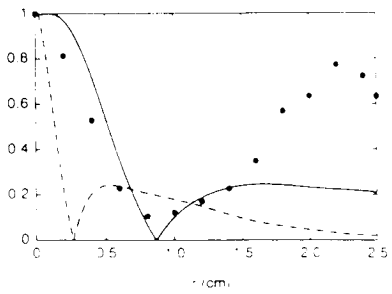

Fig. 2b L-antenna

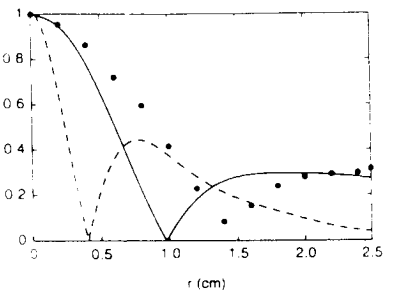

Fig. 2c P-antenna

3. RF-compensated Langmuir probes [3]. RF fluctuations in plasma potential V_s are known to distort the dc probe characteristic because of its nonlinearity. A common cure for this is to isolate the probe tip with tuned inductors, so that it can float with V_s. However, there is enough stray capacitance to ground that the probe tip does not follow V_s well enough. We use an auxiliary electrode of large area (a tungsten coil), coupled to the probe via a capacitor, to force the tip to follow oscillations in V_s. It was also necessary to use two rf chokes in series, tuned to the 27.12 MHz fundamental and its first harmonic (Fig. 3). Fig. 4 shows I-V curves in a helicon discharge taken with and without the auxiliary electrode. The correctly compensated curve shows not only a lower temperature and a higher floating potential, but also the absence of a fast electron tail. The latter has been seen by others using simpler probes but is not expected at our densities of $\geq 3 \times 10^{15}$ cm^{-3}.

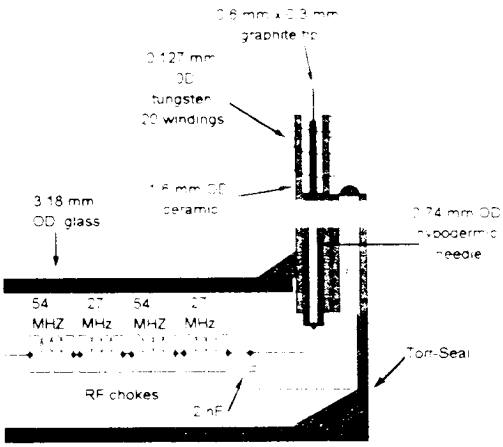

Fig. 3

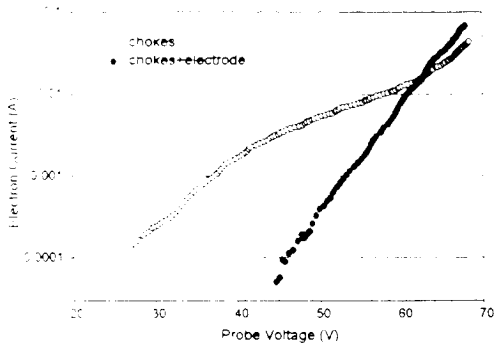

Fig. 4

4. Finite mass effects at low and high fields. Helicon waves exist in the range $\omega_{ci} << \omega << \Omega_e$, where both electron gyrations and ion motions can be neglected. At low B-fields and with light ions, the limits of this range can be approached, leading to new effects. We have found [4] a simple dispersion relation incorporating both masses:

$$\varepsilon\beta^2 - k\beta - k\alpha = 0, \quad \varepsilon \equiv \frac{\delta - \gamma}{1 - \delta\gamma} \approx \delta - \gamma, \quad \delta \equiv \frac{\Omega}{\omega + i\nu}, \quad \gamma \equiv \frac{\omega + i\nu_c}{\omega_c} \tag{3}$$

Here α is as defined in Eq. (2), and for a uniform plasma β satisfies the boundary condition

$$(\beta + k)J_{m-1}(\gamma a) - (\beta - k)J_{m+1}(\gamma a) = 0, \quad (4)$$

where $\gamma^2 = \beta^2 - k^2$. Eq. (3) shows that when either mass is finite, there are two roots β, corresponding to two types of wave. However, unless the two waves are coupled at the boundary, each must satisfy Eq. (4), hence, for given m and k, Eq. (3) yields a unique value of α, and hence of n_0, B_0. The n_0 vs. B_0 curve for argon in Fig. 5 for different m-numbers shows that the effect of electron mass is to shift the curves downwards, giving rise to a threshold magnetic field. At high fields, the ion mass causes the curves to bend upwards, but the effect is small even in helium at kilogauss fields. In neither case does the dispersion relation predict the observed density peaks seen near the electron cyclotron and lower hybrid frequencies. These are probably due to a different damping or antenna coupling mechanism.

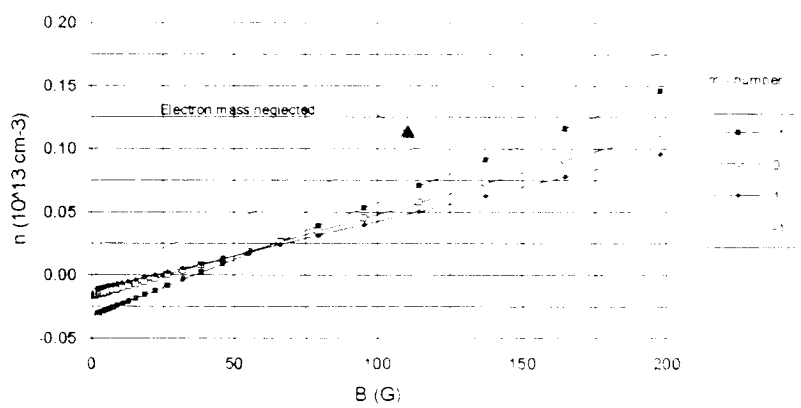

Fig. 5

5. Density enhancement techniques [5]. A factor of 5 increase in peak density and a factor of 2 increase in integrated density can be achieved by introducing a nonuniformity in the magnetic field, allowing it to flare out into a cusp behind the antenna. This causes the field lines to strike the quartz wall, forming a magnetic aperture limiter and narrowing the discharge. A similar effect can be obtained by placing a conducting or insulating material aperture limiter, with or without a central hole, behind the antenna. These beneficial effects are not yet understood, but they may be caused by the elimination of the wave energy that propagates in the wrong direction, away from the main plasma.

6. Axial variation of wave and plasma parameters. By introducing small Langmuir and magnetic probes from the end flange, we have measured the axial variation of the discharge and wave parameters over ~1 m downstream from the antenna. A small optical probe consisting of a small lens connected to an optical fiber has also been developed to measure optical emission. Fig. 6 shows the axial profiles of KT_e, n_0, and V_s (computed from the floating potential.) One sees that most of the rf energy is deposited near the antenna (at the left), and that KT_e falls from ~5 to ~2 eV downstream. The density initially rises to preserve pressure balance, then falls as the plasma diffuses to the wall. The plasma potential is constant over most of the region because of the high plasma conductivity along **B**. Fig. 7 shows the intensity of the 488 nm Ar^+ line, which is found to decay in the axial direction more slowly than the falling electron temperature would predict. The dashed curves are computed from the KT_e data assuming direct excitation and explain the initial peak. The solid curve assumes that the 488 nm line arises from the low-threshold excitation of metastable Ar^+ ions by the cool downstream electrons. The agreement is indirect evidence of the presence of metastables which are created near the antenna and subsequently drift downstream. This is confirmed by a delay in the downstream optical signal. Fig. 8 shows the magnitude variation of B_z taken with a mag-

netic probe The distance between maxima agrees with the antenna length, as expected for a

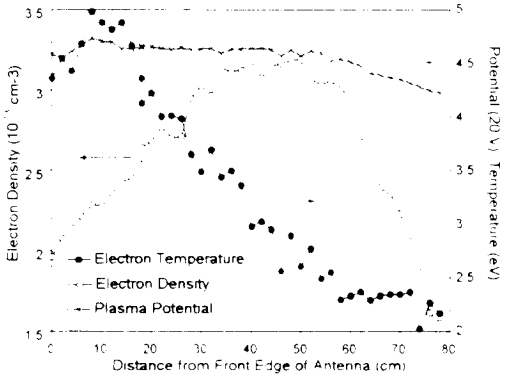

Fig. 6

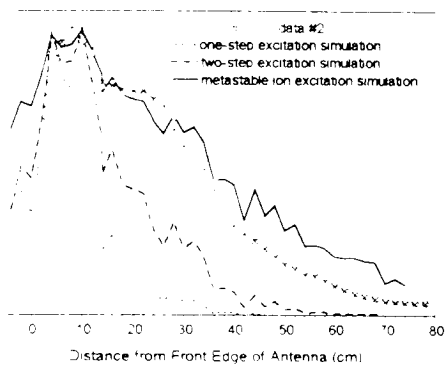

Fig. 7

half-wavelength antenna The wavelength is also seen to increase as the density decreases, as expected from Eq (2) However, since the amplitude decays to a low value at the end of the machine, the reflected wave should not be strong enough to cause a standing wave We believe, therefore, that the observed pattern is not a standing wave but the beat between two wavelengths excited simultaneously by the antenna (shaded)

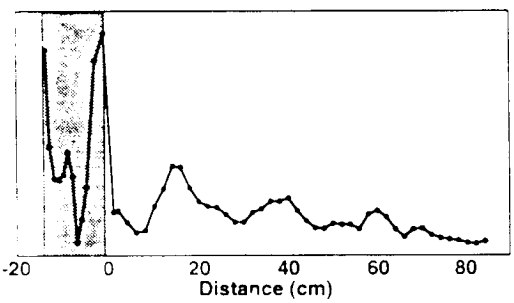

Fig. 8

7. Helicons in nonuniform magnetic fields. In plasma reactors used for etching and deposition, the magnetic field is highly nonuniform To treat this case, we have transformed the helicon equations into other coordinate systems with axes parallel to the magnetic field lines The most convenient of these are spherical coordinates, which correspond to conically diverging field lines Assuming that $n\,B$ remains constant as the plasma expands, we have found series solutions which terminate for certain angles, giving an analytic result Arbitrary field shapes can be treated by matching conical sections An example is given in Fig. 9, which gives the B_z amplitude in a parabolically diverging field for three values of $n\,B$: (A) 1.67×10^{10}, (B) 5.56×10^{9}, and (C) 3.89×10^{9} cm^{-3}/G There is qualitative agreement with experimental points [6] in that a) the wave decays by geometrical spreading, b) the wavelength increases as $n\,B$ increases, in agreement with the local dispersion relation Eq (2), and c) the wavelength decreases for constant $n\,B$ as the plasma radius increases, also in agreement with Eq (2), since $\alpha \approx T$ varies roughly as $1/a$

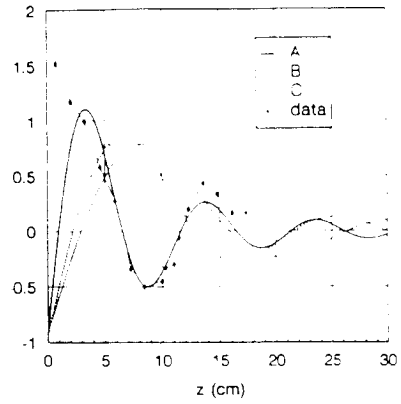

Fig. 9

1 F F Chen, M J Hsieh, and M Light, Plasma Sources Sci Technol 3, 49 (1994); I D Sudit and F F Chen, Plasma Sources Sci Technol (to be published, 1994)

2 M Light and F F Chen, Bull Amer Phys Soc **38**, 1897 (1993), to be published

3 I D Sudit and F F Chen, Plasma Sources Sci Technol 3, 162 (1994)

4 F F Chen, "Helicon Plasma Sources" Review paper in *High Density Plasma Sources*, ed by Oleg A Popov (Noyes Publications), to be published (1994)

5 G Chevalier and F F Chen, J Vac Sci Technol A **11**, 1165 (1993)

6 T Shoji, private communication